AMSE JOURNALS-AMSE IIETA publication-2017-Series: Modelling B; Vol. 86; N°1; pp 155-168
Submitted Jan. 2017; Revised March 15, 2017, Accepted April 15, 2017

Structure Analysis of a Large Water Conveyance Tunnel with Consideration of Grouting Circle Failure

Q. Yuan, Y.Z. Wang*, W.J. You, G.N. Xu

School of Civil Engineering, Shandong University, Jinan, China
Corresponding author E-mail address: 35012530@qq.com (Y.Z. Wang).

Abstract

Based on Complete Fluid-solid Coupling Theory, this paper takes permeability coefficient and void ratio as variables changing with volume strain, defines damage variables to reflect damage of surrounding rock, establishes an elastoplasticity damage constitutive model of seepage coupling of stress in surrounding rock, and then analyzes a large water conveyance tunnel in view of adverse situation of grouting circle failure. The results show that grouting circle failure has significant adverse effects on stability of surrounding rock and stress of the lining and the anchor rods.

Key words

Fluid-solid coupling, water conveyance tunnel, grouting circle failure

1. Introduction

As more and more large-scale water diversion projects in China have been constructed and put into operation, the construction of large-scale water conveyance tunnels has become a very important issue in water diversion projects and attracted more and more attention. Therefore, analysis and research of large-scale water conveyance tunnels has important theoretical and engineering significance.

Scholars domestic and abroad have done a lot of work in the calculation of large-scale water conveyance tunnels. With the development and application of the finite element method, 2d and 3d numerical analysis methods represented by the finite element method have been widely used. Current research mostly focus on waterproofing and drainage technology of tunnels [1][2], while coupling mechanism of surrounding rock stress field and seepage field is very rare [3][4],

especially on stability of surrounding rock considering fluid-solid coupling is even less [5][6]. Almost all the completed and ongoing research is based on ideal running status of tunnels and takes little consideration of adverse conditions such as grouting circle failure.

In addition, most papers on analysis of seepage field, stress field of surrounding rock and bearing characteristics of tunnel lining adopt a fluid-solid coupling calculation method which takes permeability coefficient as a constant and does not consider dynamic changes of permeability coefficient or void ratio during the process of surrounding rock excavation and water conveyance by stress, pore pressure and deformation and damage of the rock, resulting in deviation between analysis and engineering practice.

Based on complete fluid-solid coupling theory, takes permeability coefficient and void ratio as variables changing with volume strain, defines damage variable to reflect damage of surrounding rock, defines damage variables to reflect damage of surrounding rock, establishes an elastoplasticity damage constitutive model of seepage coupling of stress in surrounding rock, and then analyzes a large water conveyance tunnel in view of adverse situation of grouting circle failure. The results can not only provide technical support for practical engineering, engineering plan optimization, ensure project safety, but also provide direct engineering experience for similar projects in the future.

2. Rock Seepage Coupling Stress Theory

Traditional fluid-solid coupling researches consider permeability coefficient and void ratio to be constant. In fact, pore fluid pressure in porous media causes changes of effective stress in porous media which causes changes of permeability coefficient, porosity and so on in the seepage process. At the same time, these changes will adversely affect the flow and pressure distribution of the pore fluid. The effect of coupling of surrounding rock stress field and seepage field must be considered in the research of rock seepage.

2.1 Finite element discrete method of fluid-solid coupling

Geomaterials stress equilibrium equation:

$$\int_V \delta\varepsilon^T D_{ep} \frac{d\varepsilon}{dt} + \int_V \delta\varepsilon^T D_{ep} \left(m \frac{\left(S_w + p_w \xi\right)}{3K_S} \frac{dp_w}{dp} \right) dV -$$

$$\int_V \delta\varepsilon^T m\left(S_w + p_w \xi\right) \frac{dp_w}{dp} dV = \int_V \delta u^T \frac{df}{dt} dV + \int_V \delta u^T \frac{dt}{dt} dS$$

(1)

Dep—elastoplastic matrix.

Seepage continuous equation：

$$s_w\left(m^T-\frac{m^T D_{ep}}{3K_S}\right)\frac{d\varepsilon}{dt}-\nabla^T\left[k_0k_r\left(\frac{\nabla p_w}{\rho_w}-g\right)\right]+$$
$$\left\{\xi_n+n\frac{S_w}{K_w}+S_w\left[\frac{1-n}{3K_S}-\frac{m^T D_{ep}m}{(3K_S)^2}\right](s_w+p_w\xi)\right\}\frac{dp_w}{dt}=0$$

(2)

k_0—product of initial permeability tensor and density of water;

k_r—proportion coefficient of permeability, as the function of saturation, stress, strain and damage variables.

Shape function：

$$\begin{cases}u=N_u\bar{u}\\ \varepsilon=B\bar{u}\\ p_w=N_p\bar{p}_w\end{cases}$$

(3)

Substitute the above equation into equation (1-1) to get solid finite element equation:

$$K\frac{d\bar{u}}{dt}+C\frac{d\bar{p}_w}{dt}=\frac{df}{dt}$$

(4)

$$K=\int_V B^T D_{ep}BdV$$

(5)

$$C=\int_V B^T D_{ep}m\frac{(s_w+\xi p_w)}{3K_S}N_p dV-\int_V B^T D_{ep}(s_w+\xi p_w)mN_p dV$$

(6)

$$df=\int_V N_u^T dfdV+\int_S N_u^T dfdS$$

(7)

In the analysis of seepage field, flow boundary condition can be expressed as：

$$-n^T kk_r\left(\frac{\nabla p_w}{\rho_w}-g\right)=q_w$$

(8)

Pore pressure boundary condition can be expressed as：

$$p_w = p_{wb}$$

(9)

Galerkin method can be expressed as:

$$\int_V a^T \overline{A} dV + \int_S b^T \overline{B} dS = 0$$

(10)

Change (1-2) as $\overline{A}$ and Change (1-8) as $\overline{B}$. Substitute (1-3) into (1-10) and make *a*=-*b*:

$$E\frac{d\overline{u}}{dt} + F\overline{p}_w + G\frac{d\overline{p}_w}{dt} = \quad f$$

(11)

$$E = \int_V N_p^T \left[s_w \left(m^T - \frac{m^T D_{ep}}{3K_S} \right) B \right] dV$$

(12)

$$F = \int_V N_p^T \left(\nabla N_p \right)^T k k_r \nabla N_p dV$$

(13)

$$G = \int_V N_P^T \left\{ s_w \left[\left(\frac{1-n}{K_S} \right) - \frac{m^T D_{ep} m}{\left(3K_S\right)^2} \right] \left(s_w + p_w \xi \right) + \xi n + n \frac{s_w}{K_w} \right\} dV$$

(14)

$$f = \int_S N_p^T q_{wb} dS - \int_V \left(\nabla N_p \right)^T k k_r g dV$$

(15)

Based on the coalition of (1-4) and (1-11), seepage coupling stress equation can be expressed as:

$$\begin{bmatrix} K & C \\ E & G \end{bmatrix} \frac{d}{dt} \begin{Bmatrix} \overline{u} \\ \overline{p}_w \end{Bmatrix} + \begin{bmatrix} 0 & 0 \\ 0 & F \end{bmatrix} \begin{Bmatrix} \overline{u} \\ \overline{p}_w \end{Bmatrix} = \begin{Bmatrix} \frac{df}{dt} \\ f \end{Bmatrix}$$

(16)

2.2 Rock medium permeability evolution model

Considering the influence of temperature, Li Peichao [7] established a Fluid-solid Coupling mathematical model of complete saturated porous medium. The relationship between porosity and temperature, stress, volume strain is as follows:

$$n = 1 + \frac{(1-n_0)}{1+\varepsilon_V}(1 - \Delta p/k_s + \beta_s \Delta T)$$

(17)

Without considering temperature and volume change of skeleton particles in seepage engineering, when there is no expansion phenomenon, porosity can be expressed as:

$$n = 1\text{-}\frac{(1-n_0)}{1+\varepsilon_V} = \frac{n+\varepsilon_V}{1+\varepsilon_V}$$

(18)

When there is expansion phenomenon, the dynamic evolution porosity model in the contractive condition can be expressed as:

$$n = 1\text{-}\frac{(1-n_0)}{1-\varepsilon_V} = \frac{n-\varepsilon_V}{1-\varepsilon_V}$$

(19)

According to the Kozeny equation, the equation of the relationship between seepage coefficient and volume strain can be expressed as：

$$k = k_0 \frac{1}{1+\varepsilon_V}\left[1 + \frac{\varepsilon_V}{n_0} - \frac{(\beta_s \Delta T + \Delta p/k_s)(1-n_0)}{n_0}\right]^3$$

(20)

Without considering temperature and volume change of skeleton particles in seepage engineering, the dynamic evolution model of seepage coefficient in the isothermal seepage process can be expressed as:

$$k = k_0 \frac{1}{1+\varepsilon_V}\left(1 + \frac{\varepsilon_V}{n_0}\right)^3$$

(21)

Using the same analysis method, the dynamic evolution model of seepage coefficient in the contractive condition after dilatation can be expressed as:

$$k = k_0 \frac{1}{1-\varepsilon_V}\left(1 - \frac{\varepsilon_V}{n_0}\right)^3$$

(22)

Based on the concept of fissured rock mass dynamic evolution, the rock damage evolution concept can be expressed as:

$$\Omega=\frac{n_0-n}{n_0-n_s}$$

(23)

n_0—fissured rock mass initial porosity;

n_s—porosity when the rock mass strength reaches the limit.

Substitute (1-18), (1-19) into (1-10) respectively, damage evolution equation can be expressed as：

$$\Omega=\frac{n_0-n}{n_0-n_s}=\begin{cases}0\\ \dfrac{n_0-\dfrac{n+\varepsilon_V}{1+\varepsilon_V}}{n_0-n_s}\\ \dfrac{n_0-\dfrac{n-\varepsilon_V}{1-\varepsilon_V}}{n_0-n_s}\end{cases}$$

(24)

Equation (1-24) is fissured rock mass damage evolution equation.

Based on the effective stress principle (1-25), the incremental elastoplastic damage constitutive relation of saturated rock mass can be expressed as:

$$\sigma_{ij}^{'}=\sigma_{ij}-np\sigma_{ij}$$

(25)

$$\begin{aligned}\mathrm{d}\sigma_{ij}&=(1-\Omega)E_{ijkl}^{0}\left(\mathrm{d}\varepsilon_{kl}-\mathrm{d}\varepsilon_{kl}^{p}\right)-n\mathrm{d}p_w\delta_{ij}-\mathrm{d}np_w\delta_{ij}\\&=\frac{n-n_s}{n_0-n_s}E_{ijkl}^{0}\left(\mathrm{d}\varepsilon_{kl}-\mathrm{d}\varepsilon_{kl}^{p}\right)-n\mathrm{d}p_w\delta_{ij}-\mathrm{d}np_w\delta_{ij}\end{aligned}$$

(26)

E_{ijkl}^{0}—stiffness matrix of no damage rock mass.

3. Numerical Simulation Analysis

The large water conveyance tunnel is composed of the inlet shaft section, the bottom flat hole section and the inclined shaft section. The whole horizontal projection length of the tunnel is 532.639 m. The actual tunnel length is 585.38 m in which the inlet shaft section is 82.25m, bottom flat hole section is 307.17m and inclined shaft section is 195.96m, 20 ° slope gradient.

A typical section plane of the inlet shaft section is simulated by the plane strain seepage flow stress coupling calculating model. The surrounding rock is simulated by the Drucker-Prager constitutive model which considers permeability coefficient changing with volume strain by a subroutine of USFIELD. Surrounding rock and lining model consists of plane 4 nodes cells(CPE4RP) and rebar and anchor model consists of T2D2 link cells. Based on reference documentation and comparison of actual calculation, calculation range should be three times larger than the diameter of excavation hole. So, the calculation range is 80×82.3m consisting 1410 cells and 1592 nodes. Rock calculation parameters are chose based on the results of rock physics mechanics tests carried out in the geological memoir and calculation parameters of concrete and rebar on relevant specifications.

At first, we balance crustal stress to establish initial equilibrium state. This paper starts with static calculation (gravity stress and external load exerted only in the analysis step) to obtain stress component data, generates data file, and reaches balance of initial crustal stress. Fluid-solid coupling analysis employs transient analysis to calculate time variation of pore pressure and settlement in the change process, and reaches total pore pressure solution. The analysis of surrounding rock and structure mainly focus on grouting circle failure.

3.1 Principal stress of surrounding rock

While the digging of tunnel starts, the whole surrounding rock is in a compression situation, with the largest pressure stress at the tunnel side wall being 8.57MPa, and only small section at the tunnel bottom is under the tension situation, with the principal tension stress being 0.028MPa.

When starting water delivery into the tunnel, due to internal water pressure, the vault and bottom surrounding of the tunnel are both under compression, with a maximum tension stress of 0.165MPa, as shown in Fig 1.After the grouting circle failure occurs, and water-block curtain grouting stops functioning, maximum principal tension stress on surrounding rock of the excavation tunnel reaches 0.257MPa, 1.6 times of when grouting circle was preventing water; as internal water pressure can relieve some of the pressure on surrounding rocks, the maximum pressure stress of surrounding rock side wall drops from 8.01MPa before water delivery to 7.39MPa, as shown in Fig 2.

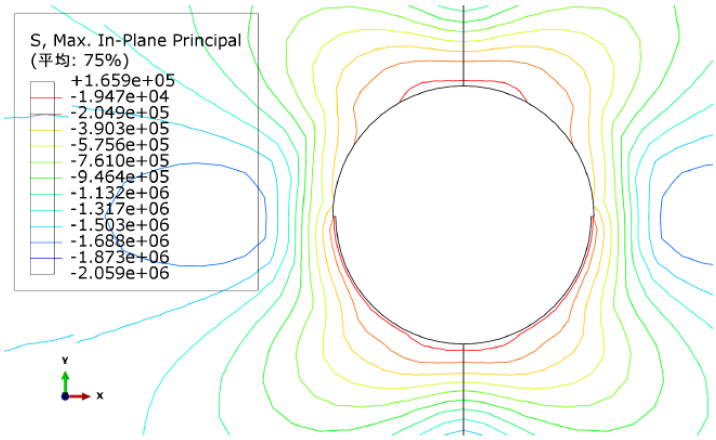

Fig 1. Contour map of maximum principal stress on surrounding rock during the period of water delivery (Unit: Pa)

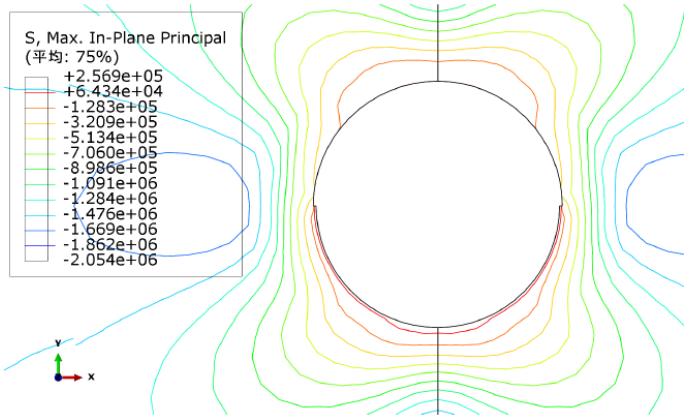

Fig 2. Contour map of maximum principal stress on surrounding rock after grouting circle fails (Unit: Pa)

Maintenance of grouting circle: after grouting circle fails, maintenance work starts and water in the tunnel are drained out. Due to relieve of inter water pressure, maximum principal stress on surrounding rock side wall reaches 7.9MPa. After re-grouting to form water-block curtain grouting, all side walls are in a compression situation, and only arch bottom in under tension stress, with a maximum principal tension stress of 0.04MPa, 6% of when grouting circle failure occurs.

Comparing the stress of different water levels in the maintenance period, we can conclude that tension stress on side walls decreases as the water level drops; when water level drops to 3/4 of tunnel diameter, the maximum principal tension stress is 0.66MPa; and when internal water are drained out, the maximum principal tension stress decreases to 0.55MPa. while compression stress on side walls increases as the water level drops; when water level drops to 3/4 of tunnel

diameter, the maximum principal compression stress is 7.34MPa; and when internal water are drained out, the maximum principal compression stress increases to 7.8MPa, as shown in Fig 3.

The analysis above indicates that principal tension stress of side walls after the failure of grouting circle reaches its maximum value of 0.254MPa during the period of water delivery, which is lower than 3MPa, class Ⅲ rock tensile strength; and principal compression stress of side walls after tunnel excavation reaches its maximum value of 8.57MPa, which is lower than 40MPa, class Ⅲ rock tensile strength. Judging from the perspectives of principal compression stress, side walls are in a safe status.

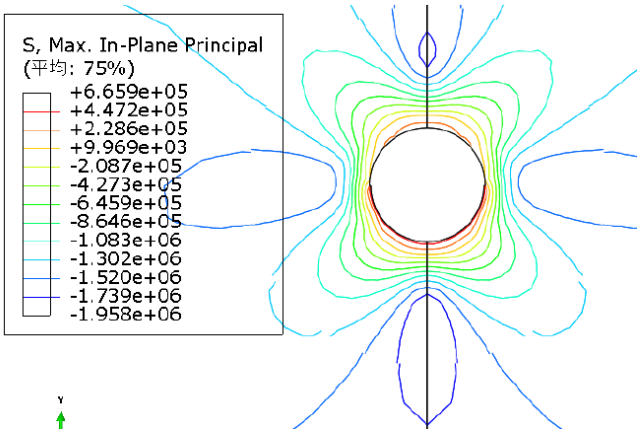

a. When water level drops to 3/4 of tunnel diameter

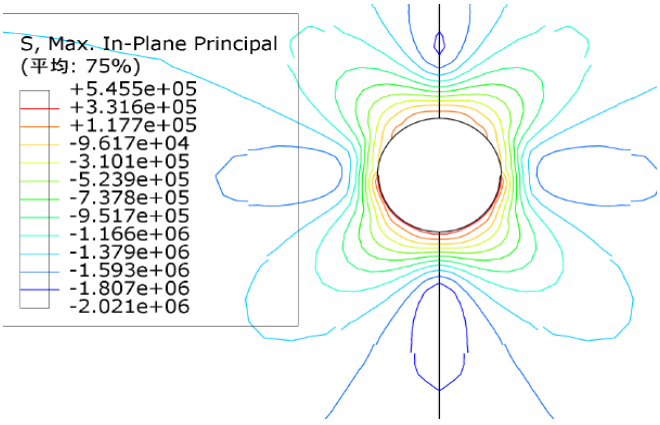

b. When internal water is drained out

Fig 3. Contour map of maximum principal stress on surrounding rock during the period of maintenance (Unit: Pa)

3.2 Seepage area of surrounding rock and lining

Under the initial condition, side walls are saturated before tunnel excavation, left, right and bottom boundary are water-proof, top and bottom hydraulic head values are hydraulic head boundary values applied in initial condition. After tunnel excavation starts, water pressure drops instantly, especially vertically. Grouting circle greatly affects pore water pressure distribution, contour lines concentrate in water-block curtain grouting and water level dramatically increases. At the beginning of water delivery, due to the effect of internal water pressure, surface water pressure in the tunnel abruptly increases, internal water exosmosis happens, but after water delivery, external water endosmosis happens. Water-block curtain grouting of grouting circle relieves effects caused by external water endosmosis. Fig 4 shows contour map of pore water pressure of surrounding rock of the excavation tunnel before and after the failure of grouting circle during the period of water delivery, and this figure also shows water-block effect of grouting circle.

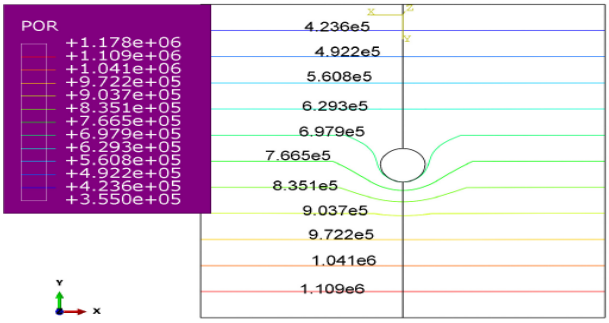

a. When grouting circle is preventing water

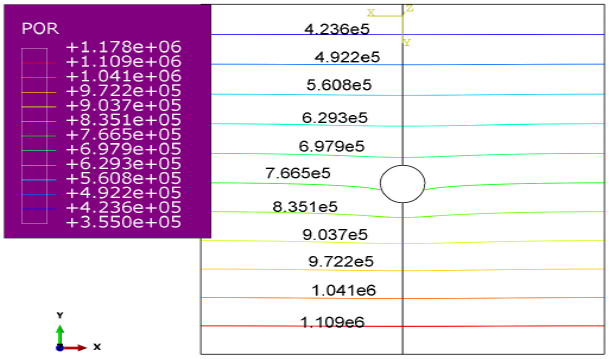

b. When grouting circle has failed

Fig 4. Contour map of pore water pressure of surrounding rock of the excavation tunnel before and after the failure of grouting circle during the period of water delivery (Unit: Pa)

Fig 5 shows contour maps of lining pore water pressure under the condition of grouting circle failure and water-block. When grouting circle fails, external water pressure on the external surface of lining is 0.623MPa, and when water-block effect recovers, external water pressure on the external surface of lining is 0.06MPa. The water-block effect of grouting circle has made outer edge of grouting circle the major structure of undertaking external water pressure, which greatly relieves pressure on lining.

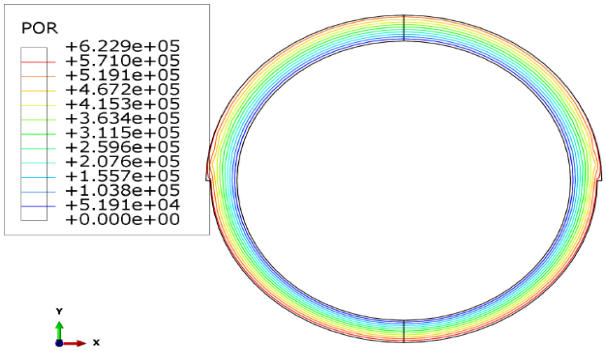

a. When grouting circle has failed

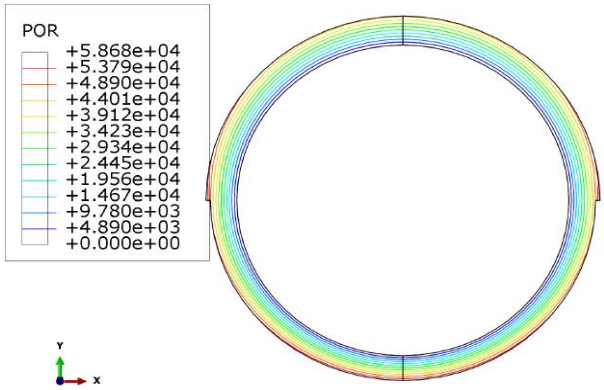

b. When grouting circle is preventing water

Fig 5. Contour maps of lining pore water pressure under the condition of grouting circle failure and water-block (Unit: Pa)

3.3 Lining principal stress

Stress changes greatly when lining is going through the period of water delivery and drainage maintenance. After lining constructions finishes, due to the seepage effect, the maximum tension stress on the outer edge of lining in contact with surrounding rock is 0.35MPa and the maximum compression stress at the lower side wall is 1.48MPa. After water delivery, due

to the internal water pressure, the maximum tension stress on the vault and arch bottom of the inner edge of lining is 1.45MPa and the maximum compression stress is 0.36MPa. It can be seen that the internal water pressure greatly relieves pressure on lining. After the grouting circle failure occurs, the position and value of the maximum stress on the lining have certain changes. Before water delivery, the maximum tension stress of the rock bolts is 15.03MPa at the upper side wall. During the period of water delivery, the maximum tension stress decreases to 13.19MPa. After failure of the grouting circle, the maximum tension stress increases to 18.07MPa.

Conclusions

Based on complete fluid-structure interaction theory, regards permeability coefficient and void ratio as variables changing with volume strain, defines damage variable to reflect damage of surrounding rock, establish a seepage coupling stress damage elastoplastic constitutive model of surrounding rock, and then analyzes a large water conveyance tunnel in view of adverse situation of failure of the grouting circle. The main conclusions are as follows:

(1) Almost all the completed and ongoing researches are based on ideal running status of tunnels and take little consideration of adverse conditions such as grouting circle failure. That could pose a safety hazard when the tunnel runs.

(2) During the period of water delivery, the maximum tension stress of the surrounding rock appears after the failure of grouting circle which is 0.257MPa and has an obvious growth than that when grouting circle was preventing water. The maximum tension stress of the surrounding rock appears after the tunnel excavation which is 8.57MPa.

(3) After the grouting circle failure occurs, the position and value of the maximum stress on the lining have certain changes. During the period of water delivery, the tension stress which rock bolts bear has a certain decrease than that when the water delivery doer not start. After the failure of grouting circle, the tension stress which rock bolts bear increases to 18.07MPa.

Therefore, the structural response of the water conveyance tunnel when grouting circle fails should be attached enough importance and scientific research.

References

1. C. Zou, Q. Luo, Z.G. Li, Control technology of Yuanliang Mountain tunnel lining crack and seepage, 2004, Modern Tunneling Technology, vol. 41, no. 5, pp. 52-57.

2. A.J. He, Waterproofing and drainage construction techniques for multi-arch tunnel partition wall, 2005, Chinese Journal of Underground Space and Engineering, vol. 1, no. 3, pp. 449-459.
3. Y.M. Lai, Z.W. Wu, Y.L Zhu, L.N. Zhu, Nonlinear analyses for the couple problem of temperature seepage and stress fields in cold region tunnels, 1999, Chinese Journal of Geotechnical Engineering, vol. 21, no. 5, pp. 529-533.
4. C. Zangerl, E.A. Eberhardt, S. Loew, Ground settlements above tunnels in fractured crystalline rock: numerical analysis of coupled hydro mechanical mechanisms, 2003, Hydrogeology Journal, vol. 16, no. 11, pp. 162-173.
5. X.M. Ji, Discussion on the research of coupled solid and fluid flow in tunnel engineering, 2006, Chinese Journal of Underground Space and Engineering, vol. 2, no. 1, pp. 149-154.
6. T.C. Li, S.C. Li, W.Z. Chen, X.B. Qiu, Coupled fluid-mechanical analysis of Xiamen Subsea Tunnel, 2004, Chinese Journal of Geotechnical Engineering, vol. 26, no. 3, pp. 397-401.
7. P.C. Li, X.Y. Kong, D.T. Lu, Mathematical modeling of flow in saturated porous media on account of fluid-structure coupling effect, 2003, Journal of Hydrodynamics, vol. 18, no. 4, pp. 419-426.
8. J. Xia, L. Xiao, L.P. Wan, Application of random-fuzzy probability statistics method, 2016, Application of Random-fuzzy Probability Statistics Method, vol. 3, no. 1, pp. 19-24.
9. B.N. Hamza, B. Said, G. Badia, T. Mohamed, Unsteady double diffusive natural convection with Dufour and Soret Effects, 2016, International Journal of Heat and Technology, vol. 34, no. 1, pp. 39-46.
10. Y. Dong, M.X. Li, Experimental study on the parameters effect on the sampling method based on negative pneumatic conveying, 2016, International Journal of Heat and Technology, vol. 34, no. 1, pp. 47-50.
11. Y.H. Madani, M. Bensaada, Heat generating couple stress fluid flow through a channel filled with a porous medium, 2013, International Journal of Heat and Technology, vol. 31, no. 1, pp. 103-108.
12. C. B. Zuada, M. A. Hicks, Numerical analysis of railway transition zones in soft soil, 2016, Proceedings of the Institution of Mechanical Engineers, Part F: Journal of Rail and Rapid Transit, vol. 230, no. 6, pp. 1601-1613.
13. E. Bombasaro, T. Kasper, Evaluation of spatial soil variability in the Pearl River Estuary using CPTU data, 2016, Soils and Foundations, vol. 56, no. 3, pp. 496-505.

14. Z. Ding, M.Y. Zhang, S.L. Li, X. J. Wei, T. N. Do, The pore pressure model of cement soil under cyclic loading, 2015, Materials Research Innovations, vol. 19, pp. 409-415.
15. E. J. Hoppe, Y. J. Kweon, B. S. Bruckno, S. T. Acton, L. Bolton, A. Becker, A. Vaccari, Historical analysis of tunnel approach displacements with satellite remote sensing, 2015, Transportation Research Record, vol. 2510, pp. 15-23.
16. V. Fargnoli, C. G. Gragnano, D. Boldini, A. Amorosi, 3D numerical modelling of soil–structure interaction during EPB tunneling, 2015, Geotechnique, vol. 65, no. 1, pp. 23-37.
17. N. Akinci, J. Cornelis, G. Akinci, M. Teschner, Coupling elastic solids with smoothed particle hydrodynamics fluid, 2013, Computer Animation and Virtual Worlds, vol. 24, no. 3-4, pp. 195-203.
18. C. Callari, F. Armero, A. Abati, Strong discontinuities in partially saturated poroplastic solids, 2010, Computer Methods in Applied Mechanics and Engineering, vol. 199, no. 23-24, pp. 1513-1535.
19. A. S. Corriols, G. Morgenthal, Vortex-induced vibrations on cross sections in tandem arrangement, 2014, Structural Engineering International: Journal of the International Association for Bridge and Structural Engineering, vol. 24, no. 1, pp. 20-26.
20. G. Q. Chen, X. T. Feng, H. Zhou, B. R. Chen, S. L. Huang, C. Q. Zhang, Numerical analysis of the long-term stability of the seepage tunnel in Jinping II Hydropower Station, 2007, Rock and Soil Mechanics, vol. 28, no. SUP, pp. 417-422.